Nanoscale Plasmon-Enhanced Spectroscopy in Memristive Switches

Giuliana Di Martino, Stefan Tappertzhofen, Stephan Hofmann, and Jeremy Baumberg**

***R**esistive switching memories are nonvolatile memory cells based on nano-ionic redox processes and offer prospects for high scalability, ultrafast write and read access, and low power consumption. In two-terminal cation based devices a nanoscale filament is formed in a switching material by metal ion migration from the anode to the cathode. However, the filament growth and dissolution mechanisms and the dynamics involved are still open questions, restricting device optimization. Here, a spectroscopic technique to optically characterize in situ the resistive switching effect is presented. Resistive switches arranged in a nanoparticle-on-mirror geometry are developed, exploiting the high sensitivity to morphological changes occurring in the tightly confined plasmonic hotspot within the switching material. The focus is on electrochemical metallization and the optical signatures detected over many cycles indicate incomplete removal of metal particles from the filament upon RESET and suggest that the filament can nucleate from different positions from cycle to cycle. The technique here is nondestructive and the measurements can be easily performed in tunable ambient conditions and with realistic cell geometries.*

1. Introduction

The progressive scaling of conventional electronics is soon approaching fundamental physical limitations and reduction of power dissipation remains the most important task in microelectronics.[1] This could be achieved if logic and memory operations were performed within the same components since more than half of the processor power is consumed by data transfer between logic and memory blocks.[2] Resistive switches (RRAMs, also known as memristive switches) are one of the most promising emerging devices for memory-in-logic operations.[3] These two-terminal devices have attracted great attention due to their high scalability, ultrafast access times, and ease of fabrication.[4] In contrast to charge based devices, the logic states (ON and OFF) in RRAMs are encoded by manipulation of nanoscale conductive filaments within a switching material. The filament formation and rupture (**Figure 1**a,b) is based on either the drift of cations (electrochemical metallization, ECM, also known as conductive bridge RAM, CBRAM), or oxygen vacancies (valence change mechanism, VCM), depending on the electrode and switching materials. Although VCM-based RRAMs offer a higher device endurance than ECM-RRAMs (with best results 10^{12} cycles for Ta_2O_5 based RRAMs[5] compared to typically $<10^6$ cycles for ECM cells[6]), the programming energy of ECM cells ($\approx$ pJ bit^{-1}) is about ten times smaller than that of VCM-RRAMs.[7] Theoretical calculations predict programming energies down to 10 fJ,[8] making ECM-RRAMs an ideal candidate for low-power memory-in-logic applications.

While the feasibility of sequential logic in passive RRAM arrays has been demonstrated,[3] the inferior device endurance of ECM-RRAMs currently hinders their

Dr. G. Di Martino, Prof. J. Baumberg
NanoPhotonics Centre
Cavendish Laboratory
University of Cambridge
Cambridge CB3 0HE, UK
E-mail: jjb12@cam.ac.uk
Dr. S. Tappertzhofen, Dr. S. Hofmann
Department of Engineering
Electrical Engineering Division
University of Cambridge
Cambridge CB3 0FA, UK
E-mail: sh315@cam.ac.uk

DOI: 10.1002/smll.201503165

www.MaterialsViews.com

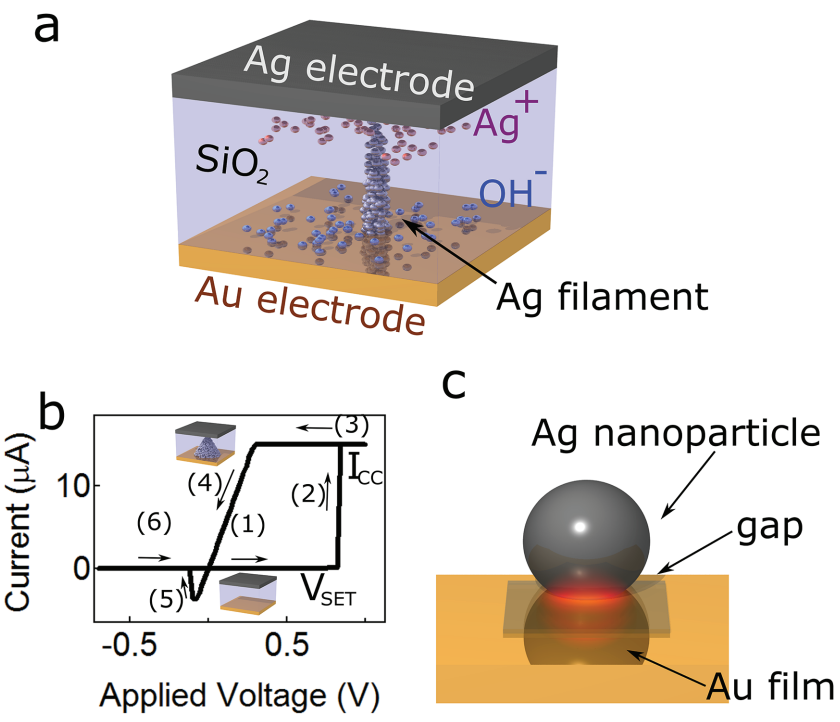

Figure 1. Memristive devices in a plasmonic geometry. a) Memristive cell based on electrochemical metallization. During switching silver cations Ag^+ are formed by anodic oxidation, while hydroxide ions OH^- act to keep charge neutrality.[16,17] b) Current–voltage (*I–V*) curve of a nanoscale $Ag/SiO_2/Au$ ECM cell (electrode 100 nm square, SiO_2 thickness 10 nm). c) Nanoparticle on mirror geometry, with plasmonic field tightly confined in the spacer material between Ag nanoparticle and Au film.

practical applications. Device optimization is however limited by their poorly understood working principle. A number of studies have recently been published on the *in situ* characterization of the switching effect using electron microscopy.[9,10] Apart from two studies which managed to record multiple switching cycles in situ,[11,12] in most such studies[13–15] only single cycles can be observed, and these typically differ significantly from what is observed under ambient conditions. For both ECM and VCM cells this can be attributed to the lack of ambient oxygen and/or moisture.[16,17] While in situ transmission electron microscopy (TEM) offers the benefit of direct observation of the filament, the sample preparation itself can result in stress and electric field gradients that differ significantly from realistic devices due to the cell geometry[11] or focused ion beam (FIB) induced damage.[18] Additionally, electrons used for imaging can perturb the movement of charged metal ions during filament formation making the interpretation of these in situ studies difficult. Recently, the shape of filaments in RRAMs has been studied by ex situ conductance atomic force tomography.[19,20] This is however a destructive technique, dependent on not modifying the ductile filaments, and by measuring the connectedness of the sample surface to the bottom electrode an inbuilt asymmetry is present while insulating filaments or particles will not be visible.[19] RRAMs have also recently been integrated into plasmonic waveguides where the filament modulates the intensity of the optical transmission across the whole structure without providing any spectral information.[21,22] However, ideally optical spectroscopy would be used instead to give detailed information about the nanometer-scale metallic configurations exactly around the filament itself and the dynamics of formation and retraction.

In this work, we present a novel spectroscopic technique to characterize in situ the resistive switching effect. We link the fields of nanoscale device engineering and plasmon-enhanced light–matter interactions by implementing optically accessible resistive switches. Local optical fields within a metal nanostructure can attain strengths that are orders of magnitude greater than the incident field. The largest field enhancements in such nanoplasmonic systems occur near sharp asperities of metal nanoparticles (NPs) and within gaps between NPs. Coinage metal dimers offer a dramatic enhancement of the induced optical field at the point of closest proximity, showing shifts of plasmon resonances toward the infrared with modes appearing and disappearing in the near-touching limit.[23] Several theoretical papers study the optical response as two nanorod ends approach and form atom-sized necks across the junction.[24,25] Particles in the near-touching limit depend sensitively on transport properties across the subnanometric metallic gaps[24,26] and a more detailed discussion is presented below. Experimental studies[27] confirm these shifts of plasmonic resonances with modes appearing and disappearing near the touching regime. However, the closely related system composed of a metal NP spaced above a metallic film is simpler to fabricate and provides exquisite control of the spacing. Using this nanoparticle-on-mirror (NPoM) geometry (Figure 1c) provides unique possibilities to study isolated plasmonic junctions reliably.[28] This geometry results in high sensitivity to morphological changes occurring in the gap (which here refers to the volume within the switching material between Ag nanodot and Au electrode), high dynamic range, and high speed interrogation. Thus, combining resistive switches and the NPoM geometry offers a powerful approach to understand the dynamics involved in the switching process.

We fabricated ECM-based resistive switches where the conductive filament is created within the plasmonic junction of an NPoM geometry (**Figure 2**a, bottom). Measurement of both electrical transport and optical scattering allows direct observation of the nanoscale kinetics of switching, opening new routes for device optimization, and thus, potentially enabling new applications. Major advantages of this technique are that it is nondestructive and that ambient conditions (atmosphere, humidity, and temperature) can be easily controlled. By using visible light we avoid electron-induced perturbation of the switching process. Since the electrical measurement setup (Figure 2a, top) is similar to standard probe station configurations, many independent switching cells can be probed without the need of sophisticated

small 2016,
DOI: 10.1002/smll.201503165

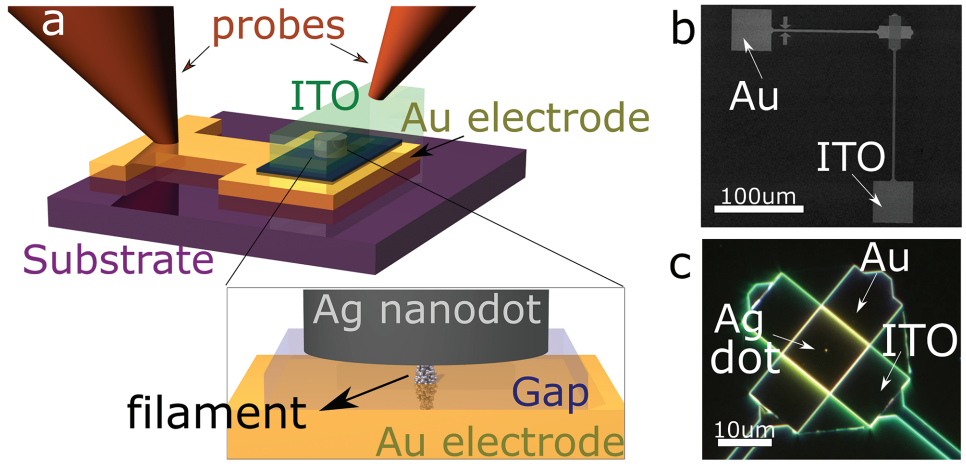

Figure 2. NPoM memristive cells. a) Sketch of sample layout, with 30 nm thick 100 nm diameter Ag-nanodot deposited on 10 nm SiO_2 spacing layer, on top of Au bottom electrode. Inset: thin filament created in the plasmonic gap. b) SEM image of the memristive cell with its Au and ITO electrodes. c) Dark field image of the memristive cell, with the Ag nanodot between the Au and ITO electrodes.

packaging and bonding. As the sample structure and fabrication used for this technique is very similar to a realistic vertical memory cell elaborate sample preparation as for transmission electron microscopy is avoided.

2. Results

We fabricated crossbar cells (Figure 2b,c) with an Au/SiO_2 layer stack and an Ag-nanodot top electrode. The 10 nm thick SiO_2 acts as switching material, while the bottom Au layer forms the counter electrode. SiO_2 was used as a model material system as it has been already widely studied[9,16,29–31] and is compatible with standard back-end-of-line (BEOL) processes.[32] The growth of Ag filaments in SiO_2 has been previously reported by in situ TEM studies.[9] For electrical connection the Ag-nanodot is connected to a large pad by an optically transparent indium-tin-oxide (ITO) layer. Since the ITO does not contribute to the switching process other conductive and optically transparent materials (such as graphene) can be used. This fabrication route allows clear observation of the NPoM scattering at the pad center through dark field spectroscopy (Figure 2c,e). Since the electrode areas of Au and ITO layers are large compared to the Ag-nanodot area (100 nm diameter), Au and ITO electrode edges do not interfere with the spectra from the nanodot. The electrochemical metallization mechanism is responsible for the switching process in this cell configuration with the filament formed by metal cations (here Ag^+[29]). We used a variable current compliance (I_{CC}) to control the current in the low resistance ON state (LRS) after the switching. For $I_{CC} \lesssim 50$ µA, the device shows multilevel switching behavior with the LRS adjustable via the I_{CC}.[30] For higher I_{CC}, the resistance of the ITO layer limits the current in the LRS. In this case, we measure a resistance of ≈ 13 kΩ for the Au/filament/Ag/ITO cell (with the filament embedded in SiO_2 layer). Resistive switching is enabled by an initial electroforming cycle where a higher voltage (typically 5–12 V) is required for the first switching.

We record the dark field scattering spectra and transient voltage and current signals simultaneously. The surface plasmons of each Ag-nanodot couple to their image charges in the gold film underneath the SiO_2 spacer layer forming a tightly confined plasmonic hotspot, similar to a nanoparticle dimer.[33,34] The optical response of this system is measured by illuminating the sample with a white light beam incident at high angle and collecting the scattered light through a dark-field objective (see the Experimental Section). The collected light is then directed to a cooled spectrometer and CCD camera.

Switching over multiple cycles after electroforming is observed with the applied voltage cycled in time (**Figure 3**a,b) in a situation where the ITO resistance limits the current in the ON state. The results are representative but the behavior for each specific cell in detail can differ. We consistently observe a change of the spectra only upon switching, but the change of intensity or peak position can vary due to the nature of the switching mechanism, involving stochastic processes and a complex interplay between electrochemical and nucleation effects among others. Using throughout a measurement range of 100 µA (to keep the integration time and sweep rate constant), the cell switches to the LRS at a SET voltage $V_{SET} \sim 0.68$ V, i.e., in the following defined as the voltage where the current abruptly changes from <10 nA (or measurement resolution) to several µA or above. Applying a negative voltage results in a RESET of the cell (switching back to the high resistance OFF state, HRS). The corresponding *in situ* scattering spectra of the Ag-nanodot show a plasmon resonance at a wavelength of $\lambda \sim 600$ nm with varying scattering amplitude (Figure 3c).

While for this device the peak position of the scattering signal remains constant, its intensity transiently doubles following switching events. Focusing on early cycles ($15\ s < t < 80\ s$) we compare the spectra to the conductance versus time (Figure 3e). After each SET event, the total conductance $G = (1/G_{RRAM} + 1/G_{ITO})^{-1}$ (where G_{RRAM} and G_{ITO} are the conductance of RRAM and ITO layers, the resistance of the Au electrode and the Ag-nanodot

DOI: 10.1002/smll.201503165

www.MaterialsViews.com

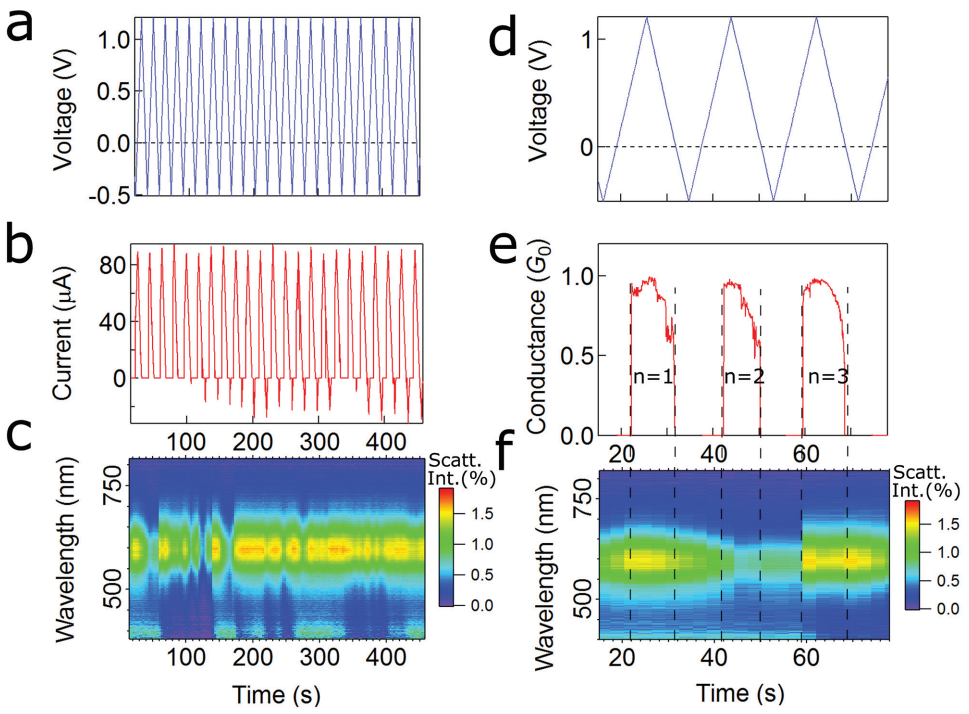

Figure 3. Multiple switching cycles in an NPoM memristive cell. a) Voltage applied to the cell. b) Corresponding measured current with c) scattering spectra. d–f) More detailed view of first three cycles $n = 1, 2, 3$ (15 s < t < 80 s) of the dataset shown in (a)–(c).

is neglected) reaches the value of one conductance quantum for an atomic point contact $G_0 = 77.5$ μS.[35,36] When a small ON-state conductance is set by the current compliance, the cell resistance is dominated by a tunnel gap between filament tip and one electrode[30] and its conductance is a tiny fraction of G_0. For relatively high conductive ON states (above G_0), a galvanic contact between the filament and the electrodes is formed, and the cell conductance is typically an integer multiple of G_0.[37] The scattering spectra simultaneously measured for these cycles (Figure 3f) show a significant increase of the peak intensity for cycles $n = 1, 3$ while the peak intensity is seen to decrease in the subsequent RESET cycles. Despite the peak intensity in the spectrum for $n = 2$ is smaller compared to the other cycles, an evident link between switching events and variation in the scattering signal can thus be observed. We believe that these changes in the scattering spectra are tightly linked to the morphological changes in the gap between the Ag–Au nano-electrodes during switching.

Figure 4 shows an electroforming cycle where we observed a remarkable impact of switching on the corresponding spectra. To highlight the dynamics the absolute cell current ($|I|$) is plotted on a logarithmic scale (Figure 4a), though to capture the large changes we used a variable current range to monitor current in both OFF and ON states. At first for t < 40 s, the cell is OFF with conductance $G < 10^{-7}$ G_0. At t > 40 s, the cell is switched to the ON state at a current compliance of $I_{CC} = 1$ μA giving a cell conductance of $G \approx 10^{-3}$ G_0 with a forming voltage of ≈ 8 V. After switching a (small) positive voltage is still applied across the cell which results in a slow increase of conductance because the driving force (positive voltage) for filament formation is reduced but not zero.[30] The fleeting resistance fluctuations (A), (B), and (C), showing transient decreases of the current in the ON state, indicate that random telegraph signal noise potentially affects the filament stability.[38] This situation has also been reported for rather high resistive ON states[39] (similar to Figure 4). At t > 70 s, the applied voltage is stepwise reduced down to 0 V. Interestingly for 86 s < t < 90 s we record negative currents although a positive voltage is applied (orange shading). Finally for t > 90 s, a negative voltage is applied between the Ag-nanodot and the Au electrode (blue shading).

The corresponding scattering spectra are mapped in Figure 4b. For t < 40 s the peak position is at $\lambda_1 \sim$ 595 nm while the intensity decreases over time, revealing that electrochemical redox reactions are already taking place in the gap between the electrodes. For t = 40 s, simultaneously with the cell current increasing by >4 orders of magnitude, we record a significant and abrupt change of the peak position (to $\lambda_1 =$ 670 nm) together with a two-fold increase of the peak intensity. The coupled plasmon peak then shifts to even higher wavelengths reaching $\lambda_1 =$ 730 nm (Figure 4c) with an additional peak emerging around $\lambda_2 =$ 500 nm upon further filament growth (40 s < t < 75 s). As discussed below, these observed spectral dynamics can be explained by the narrowing of the plasmonic junction as the cations drift from the top Ag-nanodot to the bottom Au film. As the gap size decreases, the coupling between the Ag-nanodot and its virtual image induces a red shift in the peak of the plasmon resonance wavelength tracked by the measured scattering, and the trapped field enhancement correspondingly grows. The decrease of the applied voltage is seen not only to affect the cell conductance but also the scattering spectrum of the coupled NPoM. For t > 75 s, the peak position stabilizes but the

small 2016,
DOI: 10.1002/smll.201503165

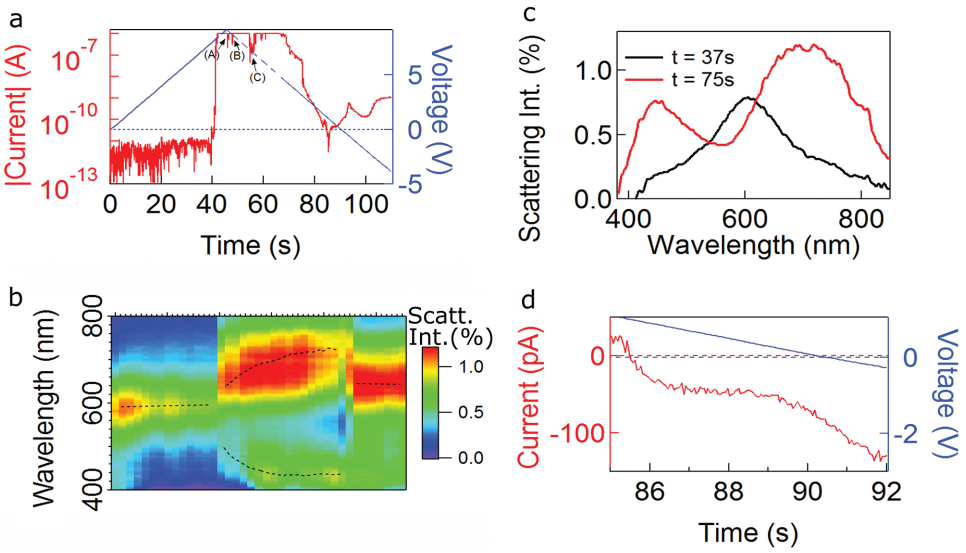

Figure 4. Electroforming cycle of NPoM memristive cell. a) Absolute value of measured current (left axis) and corresponding applied voltage (right axis). Dashed voltages differ from the actual applied voltage when current compliance is operating. Orange region corresponds to negative current at positive voltages, blue region to both current and voltage negative. The current for labels (A)–(C) correspond to filament instabilities and/or random telegraph noise. b) Scattering spectra collected simultaneously with the electrical measurements in (a). Dashed lines track peak positions. c) Detailed spectra for $t = 37$, 75 s. d) Detail of orange/blue regions in (a) between 85 s < $t = 92$ s.

intensity clearly decreases. Subsequently, the peak shifts back to a shorter wavelength when a negative voltage is applied ($t > 90$ s), at first to $\lambda_1 \approx 700$ nm and then to a stable value of $\lambda_1 = 660$ nm. The reason for this behavior is not clear but could be explained by a photocurrent and/or drift of cations or hydroxide ions (see Discussion).

3. Discussion

As discussed above, when two metallic nanostructures approach each other, shifts of plasmon resonances are observed with modes appearing and disappearing near the touching point.[23–25,27] Theoretical understanding of these systems gives useful insights linking the structural changes occurring in the memristive switching gap to their electrical and optical properties. The NPoM electrodes, the filament, and neighboring metal clusters can be considered as NPs. For large separations two NPs (e.g., the filament and the Au electrode) interact weakly, and the spectrum is dominated by a single intense mode. This so-called bonding dipolar plasmonic (BDP) resonance shows an induced charge distribution characterized by capacitive coupling of charges of opposite sign on either side of the gap.[24] As the inter-NP distance decreases, their Coulomb interaction increases and the BDP mode red shifts due to increased inter-NP coupling[23,24] The same behavior is observed in the analogous NPoM geometry, where the decreasing separation of the NP and mirror surface results in a red shift of the scattering spectrum.[26] The optical signature dramatically changes near the touching point when a transition from the capacitive to the conductive coupling regime occurs and the conductivity in the junction increases. This conductive regime is first dominated by quantum tunneling. The BDP mode is quenched and two charge transfer plasmon (CTP) modes gain intensity.[24,25] Different sizes and junction geometries investigated[25] suggest that the CTP modes merge in larger systems, in agreement with classical calculations giving a single dominant CTP mode.[27] Once the clusters are connected current flows through the whole system and the CTP intensity increases. When the two dimers are now pulled apart, as the current flowing across the junction diminishes, one of the two CTP modes converges again toward the BDP mode while the other CTP mode disappears.[24] This theoretical background (validated so far only for homo-dimers) gives insights into formation of the filament in memristive switching gaps. However, more complicated electrodynamics takes place with different metals (Au/Ag) approaching, requiring an extension of the theoretical description to connect the structural, electronic, and optical properties of these junctions.

We observe clear but nontrivial influences on the scattering spectrum of the Ag-nanodot NPoM upon switching and RESET of the cell. For reproducible switching cycles as in Figure 3b,e changes of the peak intensity following the cell switching are recorded. Below we will discuss these changes based on a simple picture of the filament (based on the electrochemical theory [4]) and potential RESET states (**Figure 5**). We suggest changes in the scattering spectra are tightly linked to the morphological changes occurring in the gap between the Ag-nanodot-Au electrodes during switching (depicted in Figure 5a,b). The measured total conductance $G \approx G_0$ indicates the presence of a galvanic contact between the filament and the electrodes[37] (Figure 5b). This should in turn result in the observation of a very strong scattering peak in the optical signal due to the presence of a CTP mode at wavelengths close to the original plasmonic peak created by near-field capacitive coupling.[27] Indeed, we experimentally detect such a strong increase of intensity, with no significant spectral shift in the scattering signal when a conductive channel is created. The measurements (Figure 3e) imply that

DOI: 10.1002/smll.201503165

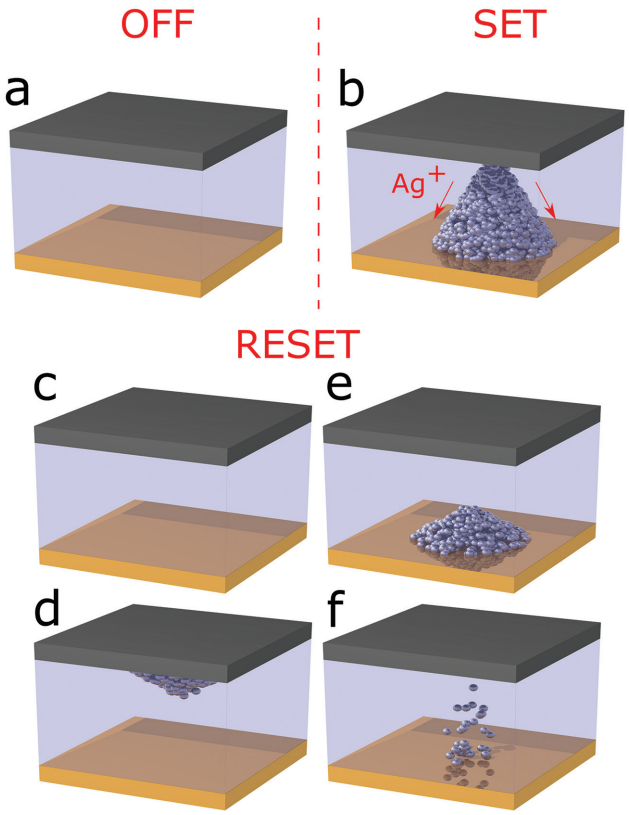

Figure 5. Filament morphologies upon SET and RESET. Different morphologies for a) an unformed cell and b) after the cell has been SET in the ON state. In this simple picture, the filament shape is determined by the drift of Ag^+ ions as indicated by arrows (based on the electrochemical theory[4]). c–f) Different filament morphologies can characterize the cell after each RESET.

the conductance of the cell in the ON state is determined by only single atoms bridging the gap between the filament tip and the opposing RRAM electrode, which in RRAM literature is termed the quantized conductance effect.[37] Characterization of this phenomenon has not yet been accessible at room temperature by any spectroscopic techniques, aside from electrical measurements.[31,40] We stress that the filament growth direction (i.e., to which electrode the filament tip galvanically bridges) is unclear. For example, the filament shape differs significantly in *in situ* TEM studies [9–12] compared to the electrochemical theory (Figure 5b). According to a simple switching model [41] the cations drift toward the Au electrode where they get reduced. After nucleation a filament is formed and further cation reduction takes place favorably at the tip of the filament due to the higher electric field. Eventually, the filament thus grows from the Au electrode toward the Ag-nanodot. However, the filament formation and the growth direction are subject to a complex interplay between the ionic redox rates and the ion mobility.[9] Moreover, the filament formation is a localized effect and statistical variations of the switching parameters are widely observed.[42] The favorable position for filament formation, the filament geometry, thickness, and growth direction may not only be different from cell to cell but may also differ from cycle to cycle depending on the previous device operation. Besides complete erasure of the filament (Figure 5c), different situations after RESET are also possible.[11] For example, the difference in spectra before electroforming and after the first RESET (Figure 4b) could be explained by a residual filament stub as depicted in Figure 5d,e. The optical signature also indicates incomplete removal of metallic particles from the filament upon RESET (Figure 5f). In this case, the peak intensity remains relatively high (higher than that of the pristine cell) both in the ON and OFF state, as shown for several cycles in Figure 3c. Note, the situations in Figures 5d–f may also co-exist. In addition, the creation of a filament at different positions underneath the Ag-nanodot affects the overall outcoupling efficiency of the light scattered by the localized plasmon into the far field, resulting in variable signal intensities. The intensity fluctuations we observe for several cycles (e.g., in Figure 3f for $n = 1,3$ and $n = 2$, respectively) thus support the view that the filament is not growing at the same position for every cycle.[12]

We want to highlight the high sensitivity of our measurement technique, which allows us to detect changes in the optical signature even for small currents close to the measurement resolution or below during RESET (e.g., Figure 3f for 32 s $\lesssim$ t $\lesssim$ 40 s and Figure 4b for $t > 70$ s). We also have evidence that changes in the optical signatures allow probing morphological changes prior to the switching/forming (e.g., Figure 4b for $t < 40$ s). These changes relate to the growth and dissolution of a filament composed of only some thousand atoms.[30]

Sometimes (as in Figure 3c) the peak intensity increases significantly after we record a higher absolute RESET current, which is typically attributed to a more stable filament.[43] A potential reason for different filament stabilities could be the precise morphology of the filament, e.g., thicker filaments or different geometrical structure within the switching material.

It is remarkable that we not only observe an influence on the spectrum when using relatively high cell currents ≈ 80 µA. Even at smaller currents < 1 µA (Figure 4) we observe pronounced impacts on the optical spectra. It is possible to observe switching upon partial growth of the Ag filament and therefore reduction of the effective distance between the electrodes without a full galvanic contact. Here, the conductive regime dominated by quantum tunneling can be explored. In this case, the thinning of the plasmonic junction in our NPoM memristive switch results in the compression of light that is now plasmonically squeezed into the nanogap. An increased intensity is observed in the plasmonic hotspots and a red shift of the plasmon evolves in the scattering spectra.[27,44] For further reduction of the gap and for conductance values in the order of G_0,[27] charge transfer screens the localized plasmon surface charge, decreasing the enhanced fields and reducing plasmonic coupling. For conductance values $G \ll G_0$ we indeed observe behavior consistent with this picture. Using this suggest that for the case in Figure 4, the early decreases in the scattering strength indicate early morphology changes or electrochemical redox reactions in the gap. Turning ON the memristive switch red shifts the peak rapidly (within our current time resolution) indicating the distance between the two electrodes is reduced due to cation migration. The additional peak emerging at $\lambda_2 = 500$ nm at the same time, which blue shifts to $\lambda_2 = 445$ nm, is likely to arise from a higher-order

DOI: 10.1002/smll.201503165

bonding mode between mixed Ag–Au dipole–quadrupole hybridized coupling.[45] Reversal of the voltage restores the plasmon spectral signature to that observed at previous times. For negative voltages a field in the opposite direction is now applied suggesting that the filament growth process is at least partially reversible with the change of peak position not simply related to irreversible changes of the switching material. One possible reason for negative currents while applying positive voltage could be the drift of cations or hydroxide ions which were not reduced during the switching process. These ions inherently induce nonequilibrium states (due to the ion distribution or different chemical activities at the electrodes) although at orders of magnitude larger current densities than reported so far.[29] Alternatively, the behavior could be explained by parasitic photocurrents generated within the RRAM. Although such behavior has not been previously reported for SiO_2 based ECM cells, the change of spectrum in both cases would underlie electrochemical redox phenomena (oxidized silver nanoparticles or cations) on the nanoscale or even on the molecular level. Such observations are validated by previous studies in which NPoM plasmonics was shown to probe morphological changes using the same measurement setup as here.[46,47]

When metallic particles remain after RESET, this is likely to continuously reduce the ON/OFF resistance window and/or the SET voltage. Different filament nucleation positions will contribute to a further accumulation of particles throughout the RRAM cell. The switching material or device operation should be thus tuned in a way that an incomplete filament dissolution is avoided. Of particular interest might be optimization or even elimination of the electroforming process where our optical signatures reveal drastic morphological changes. Moreover, defect engineering or manipulation of the electrode surfaces may allow constraining the filament to grow from a single nucleation point only.

The measurement technique presented here is not limited to ECM-RRAMs but can be used to study VCM-based cells as well. In these cells, monitoring a filament composed of an oxygen-vacancy-enriched phase within a transition metal oxide is even more difficult by in situ electron microscopy. For example, in Hf/HfO_2/Pt cells the filament is an oxygen-deficient phase within the HfO_2 film, with a different refractive index and vibrational signature. While this is difficult to observe by TEM, our technique can probe this chemical signature in the hotspot in between the two metals.[46,47] Our approach could thus be used to analyze the proposed modulation of Schottky barriers between the high work function electrode and filament stub.[4,7] We thus propose a similar NPoM geometry, with a low work function electrode (Hf or Ti) as bottom electrode, HfO_2 or TiO_2 as switching material, and an Au-nanodot as the high-work-function electrode, to probe optically SET and RESET in VCM-RRAMs.

4. Conclusions

We have presented a novel method to characterize in situ the resistive switching effect through dark field spectroscopy in an NPoM geometry. We link the fields of nanoscale device engineering and plasmon-enhanced light–matter interactions by implementing optically accessible resistive switches. The scattering signal coming from the plasmonic field which is tightly confined in the nanometer size switching gap is monitored in real time. We correlate the influence on the optical spectrum of the plasmonic hotspot present in the junction through switching and RESET cycles of the cell to the creation of a conductive channel between the electrodes, tracking as a result the morphological changes occurring in the switching material. Avoiding the impact of electron beams and a sample layout which is very similar to a realistic RRAM device are among the benefits of our technique. This results in the first in situ optical observations of the nanoscale kinetics of these switching mechanisms under ambient conditions. Our results indicate that the filament nucleation position can differ from cycle to cycle. Furthermore, the optical signal reveals an incomplete removal of filament atoms during RESET which we think will drastically affect the device endurance. Optimization of ECM-RRAMs thus needs to account for these failure mechanisms. Further experiments in variable atmosphere and/or temperature using the NPoM geometry are required to gain deeper insight into growth and dissolution of filaments. This could be complemented by in situ environmental electron microscopy[48] studies on the filament formation, taking into account the limitations arising from the cell geometry and electrons perturbing the ion movement. We also suggest the adaption of our nanophotonic technique not only for other ECM-RRAM devices but also for RRAMs based on the valance change mechanism. Our technique could also be combined with other techniques, such as electron microscopy, X-ray diffraction (XRD), or X-ray photoelectron spectroscopy (XPS), to provide powerful future metrology and correlative imaging platforms.

5. Experimental Section

Sample Fabrication: RRAM crossbars were fabricated on p-doped Si wafers with a 280 nm thick SiO_2 layer grown by wet-thermal oxidation. The bottom electrodes were deposited by thermal evaporation of 5 nm Cr (as adhesion layer) and a 30 nm Au layer (evaporation speed 0.1 nm s^{-1}). 10 nm thick SiO_2 was deposited by radio frequency (RF) sputtering in Ar atmosphere (300 W, 3.5×10^{-3} Torr = 4.7×10^{-3} hPa) as the switching material. Subsequently, 100 nm diameter large Ag-nanodots were fabricated by thermal evaporation of 30 nm Ag covered by 5 nm Cr and 30 nm Au as protective layers. This layer stack was fabricated without breaking the vacuum to avoid oxidation of the Ag-nanodot. Finally, ITO (thickness 40 nm) was deposited by direct current (DC) sputtering (50 W, 3.5×10^{-3} hPa). Electron beam lithography followed by a lift-off in Acetone and 2-Propanol were used for pattern transfer for all process steps.

Electron Microscopy: Scanning electron microscopy (SEM) images were taken using an FEI Philips XL30 sFEG SEM.

Electrical Measurements: For electrical characterization a Keithley 2635 Source meter was used in a triaxial measurement configuration, which allows low-noise measurement of currents down to 10 pA. In all measurements, the Au bottom electrode was

DOI: 10.1002/smll.201503165

grounded. A sweep rate of ≈ 0.18 V s^{-1} was used. All measurements were performed in air at room temperature.

Optical Setup: Plasmon resonances of Ag NPs were characterized by scattering spectra and color images. The sample was illuminated by high-angle white light incident through a 100× DF 0.8 NA objective (LMPlanFL N) in an optical dark field configuration. The same objective was used for collection of scattering spectra and images. The dark field scattered light was then sent to a CCD camera (Infinity) and spectrometer (Ocean Optics QE65000) for spectral analysis. Spectral content of the scattered light was measured with 3 s integration time.

Source data can be found at https://www.repository.cam.ac.uk/handle/1810/252759.

Acknowledgements

G.D.M. and S.T. contributed equally to this work. The authors acknowledge Alan Sanders for developing the data collection software and Richard Bowman for providing part of the experimental equipment. The authors acknowledge funding from ERC grant LINASS 320503, EPSRC grant EP/L027151/1, and ERC grant InsituNANO 279342.

[1] S. Kakaç, L. L. Vasiliev, Y. Bayazitoglu, Y. Yener, *Microscale Heat Transfer Fundamentals and Applications*, Springer, Dordrecht, The Netherlands, **2005**.
[2] D. A. B. Miller, *Proc. IEEE* **2009**, *97*, 1166.
[3] A. Siemon, T. Breuer, N. Aslam, S. Ferch, W. Kim, J. van den Hurk, V. Rana, S. Hoffmann Eifert R. Waser, S. Menzel, E. Linn, *Adv. Funct. Mater.* **2015**, *25*, 6414.
[4] Y. Yang, W. Lu, *Nanoscale* **2013**, *5*, 10076.
[5] M.-J. Lee, C. B. Lee, D. Lee, S. R. Lee, M. Chang, J. H. Hur, Y.-B. Kim, C.-J. Kim, D. H. Seo, S. Seo, U.-I. Chung, I.-K. Yoo, K. Kim, *Nat. Mater.* **2011**, *10*, 625.
[6] M. Kund, G. Beitel, C.-U. Pinnow, T. Rohr, J. Schumann, R. Symanczyk, K.-D. Ufert, G. Muller, *Proc. IEEE IEDM* **2005**, 754.
[7] D. J. Wouters, R. Waser, M. Wuttig, *Proc. IEEE* **2015**, *103*, 1274.
[8] D. Ielmini, *Proc. IEEE IEDM* **2011**, 17.2.1.
[9] Y. Yang, P. Gao, L. Li, X. Pan, S. Tappertzhofen, S. Choi, R. Waser, I. Valov, W. D. Lu, *Nat. Commun.* **2014**, *5*, 4232.
[10] K. D'Aquila, Y. Liu, H. Iddir, A. K. Petford-Long, *Phys. Status Solidi RRL* **2015**, *9*, 301.
[11] W. A. Hubbard, A. Kerelsky, G. Jasmin, E. R. White, J. Lodico, M. Mecklenburg, B. C. Regan, *Nano Lett.* **2015**, *15*, 3983.
[12] M. Kudo, M. Arita, Y. Ohno, Y. Takahashi, *Appl. Phys. Lett.* **2014**, *105*, 173504.
[13] Q. Liu, J. Sun, H. Lv, S. Long, K. Yin, N. Wan, Y. Li, L. Sun, M. Liu, *Adv. Mater.* **2012**, *24*, 1844.
[14] M. Kudo, M. Arita, Y. Ohno, T. Fujii, K. Hamada, Y. Takahashi, *Thin Solid Films* **2013**, *533*, 48.
[15] S.-J. Choi, G.-S. Park, K.-H. Kim, S. Cho, W.-Y. Yang, X.-S. Li, J.-H. Moon, K.-J. Lee, K. Kim, *Adv. Mater.* **2011**, *23*, 3272.
[16] S. Tappertzhofen, I. Valov, T. Tsuruoka, T. Hasegawa, R. Waser, M. Aono, *ACS Nano* **2013**, *7*, 6396.
[17] F. Messerschmitt, M. Kubicek, J. L. M. Rupp, *Adv. Funct. Mater.* **2015**, *25*, 5117.
[18] J. Mayer, L. A. Giannuzzi, T. Kamino, J. Michael, *MRS Bull.* **2007**, *32*, 400.
[19] M. Buckwell, L. Montesi, S. Hudziak, A. Mehonic, A. J. Kenyon, *Nanoscale* **2015**, *7*, 18030.
[20] U. Celano, L. Goux, R. Degraeve, A. Fantini, O. Richard, H. Bender, M. Jurczak, W. Vandervorst, *Nano Lett.* **2015**, *15*, 12, 7970.
[21] A. Emboras, J. Niegemann, P. Ma, C. Haffner, M. Luisier, C. Hafner, T. Schimmel, J. Leuthold, *ArXiv 150807748 Phys.* **2015**.
[22] A. Emboras, I. Goykhman, B. Desiatov, N. Mazurski, L. Stern, J. Shappir, U. Levy, *Nano Lett.* **2013**, *13*, 6151.
[23] I. Romero, J. Aizpurua, G. W. Bryant, F. J. G. D. Abajo, *Opt. Express* **2006**, *14*, 9988.
[24] F. Marchesin, P. Koval, M. Barbry, J. Aizpurua, D. Sanchez-Portal, *ArXiv150907194 Cond-Mat* **2015**.
[25] T. P. Rossi, A. Zugarramurdi, M. J. Puska, R. M. Nieminen, *ArXiv150901140 Cond-Mat Physicsphysics* **2015**.
[26] F. Benz, B. De Nijs, C. Tserkezis, R. Chikkaraddy, D. O. Sigle, L. Pukenas, S. D. Evans, J. Aizpurua, J. J. Baumberg, *Opt. Express* **2015**, DOI: 10.1364/OE.23.033253.
[27] K. J. Savage, M. M. Hawkeye, R. Esteban, A. G. Borisov, J. Aizpurua, J. J. Baumberg, *Nature* **2012**, *491*, 574.
[28] C. Ciraci, R. T. Hill, J. J. Mock, Y. Urzhumov, A. I. Fernandez-Dominguez, S. A. Maier, J. B. Pendry, A. Chilkoti, D. R. Smith, *Science* **2012**, *337*, 1072.
[29] I. Valov, E. Linn, S. Tappertzhofen, S. Schmelzer, J. van den Hurk, F. Lentz, R. Waser, *Nat. Commun.* **2013**, *4*, 1771.
[30] S. Menzel, U. Böttger, R. Waser, *J. Appl. Phys.* **2012**, *111*, 014501.
[31] A. Mehonic, A. Vrajitoarea, S. Cueff, S. Hudziak, H. Howe, C. Labbé, R. Rizk, M. Pepper, A. J. Kenyon, *Sci. Rep.* **2013**, *3*, 2708.
[32] Y. Bernard, V. T. Renard, P. Gonon, V. Jousseaume, *Microelectron. Eng.* **2011**, *88*, 814.
[33] P. K. Aravind, H. Metiu, *Surf. Sci.* **1983**, *124*, 506.
[34] P. Nordlander, E. Prodan, *Nano Lett.* **2004**, *4*, 2209.
[35] K. Terabe, T. Hasegawa, T. Nakayama, M. Aono, *Nature* **2005**, *433*, 47.
[36] N. Agraït, A. L. Yeyati, J. M. van Ruitenbeek, *Phys. Rep.* **2003**, *377*, 81.
[37] S. Tappertzhofen, I. Valov, R. Waser, *Nanotechnology* **2012**, *23*, 145703.
[38] D. Ielmini, F. Nardi, C. Cagli, *Appl. Phys. Lett.* **2010**, *96*, 053503.
[39] M.-C. Wu, W.-Y. Jang, C.-H. Lin, T.-Y. Tseng, *Semicond. Sci. Technol.* **2012**, *27*, 065010.
[40] T. Tsuruoka, T. Hasegawa, K. Terabe, M. Aono, *Nanotechnology* **2012**, *23*, 435705.
[41] S. Menzel, S. Tappertzhofen, R. Waser, I. Valov, *Phys. Chem. Chem. Phys.* **2013**, *15*, 6945.
[42] M. Zhang, S. Long, G. Wang, R. Liu, X. Xu, Y. Li, D. Xu, Q. Liu, H. Lv, E. Miranda, J. Suñé, M. Liu, *Nanoscale Res. Lett.* **2014**, *9*, 694.
[43] D. Kamalanathan, U. Russo, D. Ielmini, M. N. Kozicki, *IEEE Electron Device Lett.* **2009**, *30*, 553.
[44] F. Benz, C. Tserkezis, L. O. Herrmann, B. de Nijs, A. Sanders, D. O. Sigle, L. Pukenas, S. D. Evans, J. Aizpurua, J. J. Baumberg, *Nano Lett.* **2015**, *15*, 669.
[45] F. Chen, N. Alemu, R. L. Johnston, *AIP Adv.* **2011**, *1*, 032134.
[46] D. O. Sigle, J. Mertens, L. O. Herrmann, R. W. Bowman, S. Ithurria, B. Dubertret, Y. Shi, H. Y. Yang, C. Tserkezis, J. Aizpurua, J. J. Baumberg, *ACS Nano* **2015**, *9*, 825.
[47] R. W. Taylor, F. Benz, D. O. Sigle, R. W. Bowman, P. Bao, J. S. Roth, G. R. Heath, S. D. Evans, J. J. Baumberg, *Sci. Rep.* **2014**, *4*, 5940.
[48] S. Takeda, H. Yoshida, *Microscopy* **2013**, *62*, 193.

Received: October 19, 2015
Revised: November 23, 2015
Published online:

DOI: 10.1002/smll.201503165